

Deficiency of Asparagine Synthetase Causes Congenital Microcephaly and a Progressive Form of Encephalopathy

Elizabeth K. Ruzzo,^{1,25} José-Mario Capo-Chichi,^{2,25} Bruria Ben-Zeev,^{3,4,25} David Chitayat,^{5,6} Hanqian Mao,⁷ Andrea L. Pappas,⁸ Yuki Hitomi,¹ Yi-Fan Lu,¹ Xiaodi Yao,¹ Fadi F. Hamdan,² Kimberly Pelak,¹ Haike Reznik-Wolf,^{4,9} Ifat Bar-Joseph,^{3,4,9} Danit Oz-Levi,¹⁰ Dorit Lev,^{4,11,12} Tally Lerman-Sagie,^{4,12,13} Esther Leshinsky-Silver,^{4,12,14} Yair Anikster,^{3,4} Edna Ben-Asher,¹⁰ Tsviya Olender,¹⁰ Laurence Colleaux,¹⁵ Jean-Claude Décarie,¹⁶ Susan Blaser,¹⁷ Brenda Banwell,¹⁸ Rasesh B. Joshi,⁸ Xiao-Ping He,⁸ Lysanne Patry,² Rachel J. Silver,⁶ Sylvia Dobrzeniecka,¹⁹ Mohammad S. Islam,²⁰ Abul Hasnat,²⁰ Mark E. Samuels,² Dipendra K. Aryal,²¹ Ramona M. Rodriguiz,²¹ Yong-hui Jiang,²² William C. Wetsel,^{21,23} James O. McNamara,⁸ Guy A. Rouleau,^{19,24} Debra L. Silver,⁷ Doron Lancet,¹⁰ Elon Pras,^{3,9} Grant A. Mitchell,² Jacques L. Michaud,^{2,26,*} and David B. Goldstein^{1,26,*}

¹Center for Human Genome Variation, Duke University School of Medicine, Durham, NC 27708, USA

²Sainte-Justine Hospital Research Center, Montreal, QC H3T 1C5, Canada

³Edmond and Lily Safra Children's Hospital, Sheba Medical Center, 52621 Ramat Gan, Israel

⁴The Sackler School of Medicine, Tel Aviv University, 69978 Tel Aviv, Israel

⁵The Hospital for Sick Children, Division of Clinical and Metabolic Genetics, University of Toronto, Toronto, ON M5G 2L3, Canada

⁶Mount Sinai Hospital, The Prenatal Diagnosis and Medical Genetics Program, University of Toronto, Toronto, ON M5G 1Z5, Canada

⁷Molecular Genetics and Microbiology and The Duke Institute for Brain Sciences

⁸Department of Neurobiology

Duke University, Durham, NC 27708, USA

⁹The Danek Gertner Institute of Human Genetics, Sheba Medical Center, 52621 Ramat Gan, Israel

¹⁰Department of Molecular Genetics, Weizmann Institute of Science, 76100 Rehovot, Israel

¹¹Institute of Medical Genetics

¹²Metabolic Neurogenetic Clinic

¹³Pediatric Neurology Unit

¹⁴Molecular Genetics Laboratory

Wolfson Medical Center, 58100 Holon, Israel

¹⁵Hôpital Necker-Enfants Malades, 75015 Paris, France

¹⁶Department of Medical Imaging, Sainte-Justine Hospital, Montreal, QC H3T 1C5, Canada

¹⁷Department of Medical Imaging, The Hospital for Sick Children, University of Toronto, Toronto, ON M5G 2L3, Canada

¹⁸Division of Neurology, The Children's Hospital of Philadelphia, Philadelphia, PA 19104, USA

¹⁹Research Center, Centre Hospitalier de l'Université de Montréal, Montreal, QC H2L 2W5, Canada

²⁰Department of Clinical Pharmacy & Pharmacology, Faculty of Pharmacy, University of Dhaka, 1000 Dhaka, Bangladesh

²¹Department of Psychiatry and Behavioral Sciences, Mouse Behavioral and Neuroendocrine Analysis Core Facility, Duke University, Durham, NC 27710, USA

²²Department of Pediatrics and Neurobiology, Duke University School of Medicine, Durham, NC 27710, USA

²³Department of Cell Biology and Neurobiology, Duke University, Durham, NC 27710, USA

²⁴Montreal Neurological Institute, McGill University, Montreal, Quebec, Canada, H3A 2B4

²⁵These authors contributed equally to this work

²⁶These authors contributed equally to this work

*Correspondence: jacques.michaud@recherche-ste-justine.qc.ca (J.L.M.), d.goldstein@duke.edu (D.B.G.)

<http://dx.doi.org/10.1016/j.neuron.2013.08.013>

SUMMARY

We analyzed four families that presented with a similar condition characterized by congenital microcephaly, intellectual disability, progressive cerebral atrophy, and intractable seizures. We show that recessive mutations in the *ASNS* gene are responsible for this syndrome. Two of the identified missense mutations dramatically reduce *ASNS* protein abundance, suggesting that the mutations cause loss of function. Hypomorphic *Asns* mutant mice have structural brain abnormalities, including

enlarged ventricles and reduced cortical thickness, and show deficits in learning and memory mimicking aspects of the patient phenotype. *ASNS* encodes asparagine synthetase, which catalyzes the synthesis of asparagine from glutamine and aspartate. The neurological impairment resulting from *ASNS* deficiency may be explained by asparagine depletion in the brain or by accumulation of aspartate/glutamate leading to enhanced excitability and neuronal damage. Our study thus indicates that asparagine synthesis is essential for the development and function of the brain but not for that of other organs.

INTRODUCTION

Intellectual disability (ID) affects 2%–3% of the general population and is characterized by a broad range of cognitive deficits. It is usually subdivided into syndromic and nonsyndromic forms, depending on whether additional abnormalities are found. Syndromic ID is often accompanied by microcephaly, defined by a head circumference more than two SDs below the age- and sex-adjusted mean. The incidence of microcephaly, as reported in birth defect registries world-wide, varies from 1 to 150 per 100,000 depending upon the range of SD used to define microcephaly and the ethnic population. For example, microcephaly is more prevalent in populations with a high degree of consanguinity (Mahmood et al., 2011). Causes of congenital microcephaly include metabolic disorders, chromosomal anomalies, and intra-uterine infections. However, with the exception of autosomal recessive primary microcephaly (MCPH), the genetic etiology of most congenital microcephaly cases is unknown.

We ascertained four families with a distinct form of severe encephalopathy associated with congenital microcephaly and progressive brain atrophy. Two families were from the same ethnic group, whereas the other two families were independently recognized as presenting with an identical syndrome. Both pairs of families were analyzed independently by exome sequencing. Here we report the clinical features of the affected children and demonstrate that the observed phenotype in all four families can be explained by autosomal recessive deficiency of asparagine synthetase (ASNS).

RESULTS

Identification and Validation of ASNS Mutations

We identified a total of nine children from four families with a severe form of intellectual disability (Table 1; Figure 1A; Supplemental Experimental Procedures available online). These children were born with a small head circumference and showed progressive microcephaly. Although congenital microcephaly is a consistent feature of this syndrome, the patients do not fit the definition of primary microcephaly (MCPH) (Supplemental Experimental Procedures). Their clinical course was characterized by profound developmental delay and, in a majority of cases, early-onset intractable seizures (Table 1; Figure 2; Figure S1). Clinical examination revealed axial hypotonia with severe appendicular spasticity in all cases. All affected siblings of family C also showed excessive startle reflex, mimicking hyperekplexia. In addition, several affected individuals from families C and D had episodes of hypothermia. Brain MRI first performed in early infancy showed decreased cerebral volume and size of pons, presumably caused by hypodevelopment and/or atrophy, as well as delayed myelination (Figure 2; Figure S1). Some patients also showed gyral simplification. The affected children from two families (C and D) died during the first year of life because of pulmonary aspiration secondary to severe neurological dysfunction, whereas the affected individuals from the other families survived into their third decade.

Families A and B are unrelated but are both of Iranian Jewish ancestry. Targeted exonic regions were captured and sequenced in one affected individual from family A (A.II.1) and

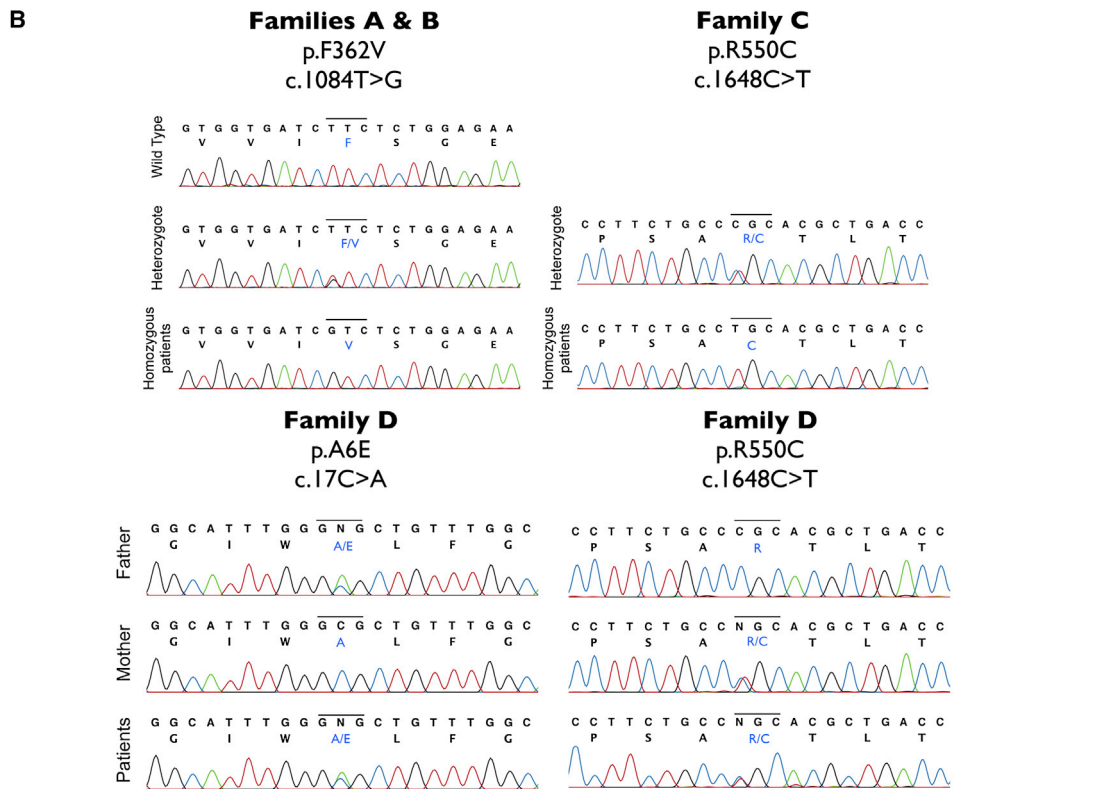
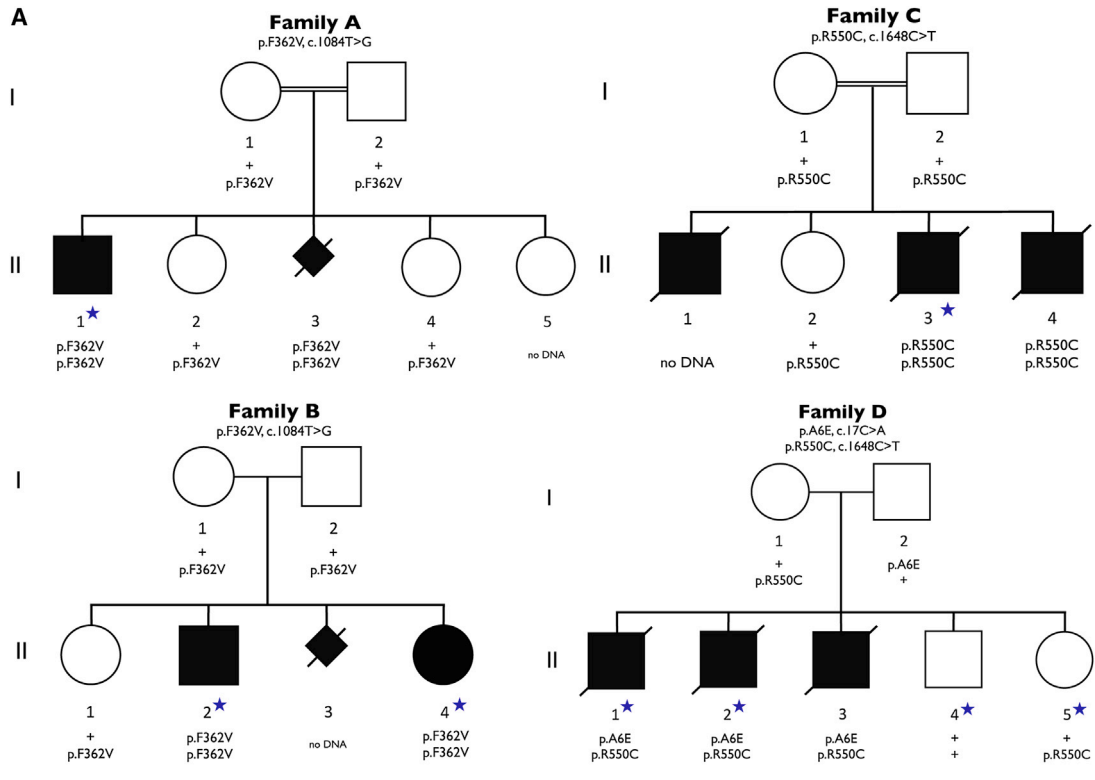
two from family B (B.II.2 and B.II.4). We focused on variants that were annotated as having a plausible impact on the function of the resulting gene product (e.g., missense, nonsense, splice site, intron-exon boundary, and coding-disrupting insertion-deletions [indels]). We compared patient exomes to control exomes sequenced in the same facility ($n = 261$, unrelated samples, not enriched for neurological disorders). Because families A and B belong to the same ethnic community and were the only similar cases identified in Israel to date, we postulated that the causal variant would be a founder mutation in this population shared among all affected individuals in these families. We therefore first focused on homozygous variants that were shared by both siblings in family B (Figure 1A, B.II.2 and B.II.4) and that were uncommon in our control population (Table S1). Since the incidence of this disorder is very low in the general population, we inspected only variants with a predicted frequency of $\leq 3\%$ in our sequenced control genomes. We found 72 such variants, only three of which were absent in the control population (Table S2). Furthermore, only one of these three variants was also present in homozygous form in the patient from family A (Figure 1A, A.II.1). This variant, located in the asparagine synthetase (ASNS) gene, causes a missense change (c.1084T > G) resulting in a phenylalanine to valine substitution at amino acid position 362 (p.F362V; NM_183356). We also performed homozygosity mapping. We found that p.F362V lies in the largest homozygous region and found no additional candidates of interest in the homozygous regions (Supplemental Experimental Procedures; Tables S7–S9).

Family C is composed of three affected (C.II.1, C.II.3, and C.II.4) siblings and one healthy (C.II.2) sibling born to consanguineous parents of Bangladeshi origin (Figure 1A). No DNA was available for the first affected child (C.II.1) who had the same clinical manifestations as his affected brothers. Homozygosity mapping showed that the two affected siblings share a total of eight homozygous regions that are >1 Mb in size (Table S3). Exome sequencing performed in one of the affected children (C.II.3) identified 856 rare protein or splice-altering variants (with a frequency $\leq 3\%$ in 169 in-house unrelated exomes, 1,000 Genomes Project data set and data from the National Heart, Lung, and Blood Institute [NHLBI] Exome Sequencing Project [ESP]). These included three variants that map to the shared regions of homozygosity; the three variants were Sanger sequenced and all three variants were homozygous in both affected individuals. The parents and the unaffected sibling were heterozygous for two of these variants, whereas the other candidate variant was excluded from further consideration because it was found in a homozygous form in one of the parents. One of the remaining variants, c.1282G > A (p.D428N; NM_017460) in the *CYP3A4* gene, is not predicted to affect protein function by SIFT or Polyphen-2 (Adzhubei et al., 2010; Ng and Henikoff, 2003) and *CYP3A4* encodes a component of cytochrome P450 (subfamily 3A, polypeptide 4), which is predominantly expressed in the liver. Thus, the *CYP3A4* variant seemed unlikely to be responsible for this phenotype. The sole remaining variant in this family is c.1648C > T (p.R550C; NM_183356) in *ASNS*, which is present in the largest region of homozygosity (35 Mb) shared by the two affected children (Table S4).

Table 1. Clinical Features of Patients with Mutations in ASNS

| | Family A | | Family B | | Family C | | Family D | | |
|-----------------------------|--|--|--|-------------------------|-------------------------|-------------------------|---------------------|--------------------------|------------------------------------|
| Consanguinity | Yes | | No | | Yes | | No | | |
| Ethnic origin | Iranian Jews | | Iranian Jews | | Bangladeshi | | French Canadian | | |
| Subjects | A.II.1 | B.II.2 | B.II.4 | C.II.1 | C.II.3 | C.II.4 | D.II.1 | D.II.2 | D.II.3 |
| Genotype | p.F362V/p.F362V | p.F362V/p.F362V | p.F362V/p.F362V | Not determined | p.R550C/ p.R550C | p.R550C/ p.R550C | p.A6E/p.R550C | p.A6E/p.R550C | p.A6E/p.R550C |
| Gender | Male | Male | Female | Male | Male | Male | Male | Male | Male |
| Age | 14 years | 14 years | 12 years | 4 months [†] | 3 months [†] | 6 months [†] | 9 days [†] | 11 months [†] | 12 months [†] |
| HC ¹ at birth | 31.5 cm (−2.5 SD) | 31 cm (−3 SD) | 31 cm (−2 SD/−3 SD) | 30.5 cm (−3.5 SD) | 33 cm (−1 SD/−2 SD) | 32 cm (−2 SD) | 31.5 cm (−2.5 SD) | 31 cm (−3 SD) | 28.5 cm (−1 SD/−2 SD) ² |
| Developmental delay | Severe | Severe | Severe | Severe | Severe | Severe | Severe | Severe | Severe |
| Progressive microcephaly | Yes | Yes | Yes | Yes | Yes | Yes | NA | Yes | Yes |
| Epilepsy | | | | | | | | | |
| Age at onset | 1 month | 2 weeks | 3 weeks | None | None | None | 4 days | 9 months ⁵ | 8 days |
| Type of seizures | Spasms, tonic, myoclonic, GTC ³ | Spasms, tonic, myoclonic, GTC ³ | Spasms, tonic, myoclonic, GTC ³ | None | None | None | Tonic, orobuccal | Partial complex | Partial complex |
| EEG pattern | Hypsarrythmia, MISF ⁴ | Hypsarrythmia, MISF ⁴ | Hypsarrythmia, MISF ⁴ | Disorganized background | Disorganized background | Disorganized background | NA | Suppression bursts, MISF | Suppression bursts, MISF |
| Clinical examination | | | | | | | | | |
| Axial hypotonia | No | No | No | No | Yes | Yes | Yes | Yes | Yes |
| Appendicular hypertonia | Yes | Yes | Yes | Yes | Yes | Yes | Yes | Yes | Yes |
| Hyperreflexia | Yes | Yes | Yes | Yes | Yes | Yes | Yes | Yes | Yes |
| Hyperekplexia | No | No | No | Yes | Yes | Yes | No | No | No |
| Brain MRI | | | | | | | | | |
| Decreased cerebral volume | Yes | Yes | Yes | Yes | Yes | Yes | Yes | Yes | Yes |
| Decreased size of pons | No | No | No | Yes | Yes | Yes | Yes | Yes | Yes |
| simplified gyri | No | No | No | Yes | Yes | Yes | Yes | Yes | Yes |

[†]Deceased; ¹head circumference; ²born at 33.5 weeks of gestation; ³generalized tonic-clonic seizures; ⁴multiple independent spike foci; ⁵tremulous movements and abnormal EEG at 4 days; partial complex seizures with eye deviation and focal epileptic activity at 9 months.



(legend on next page)

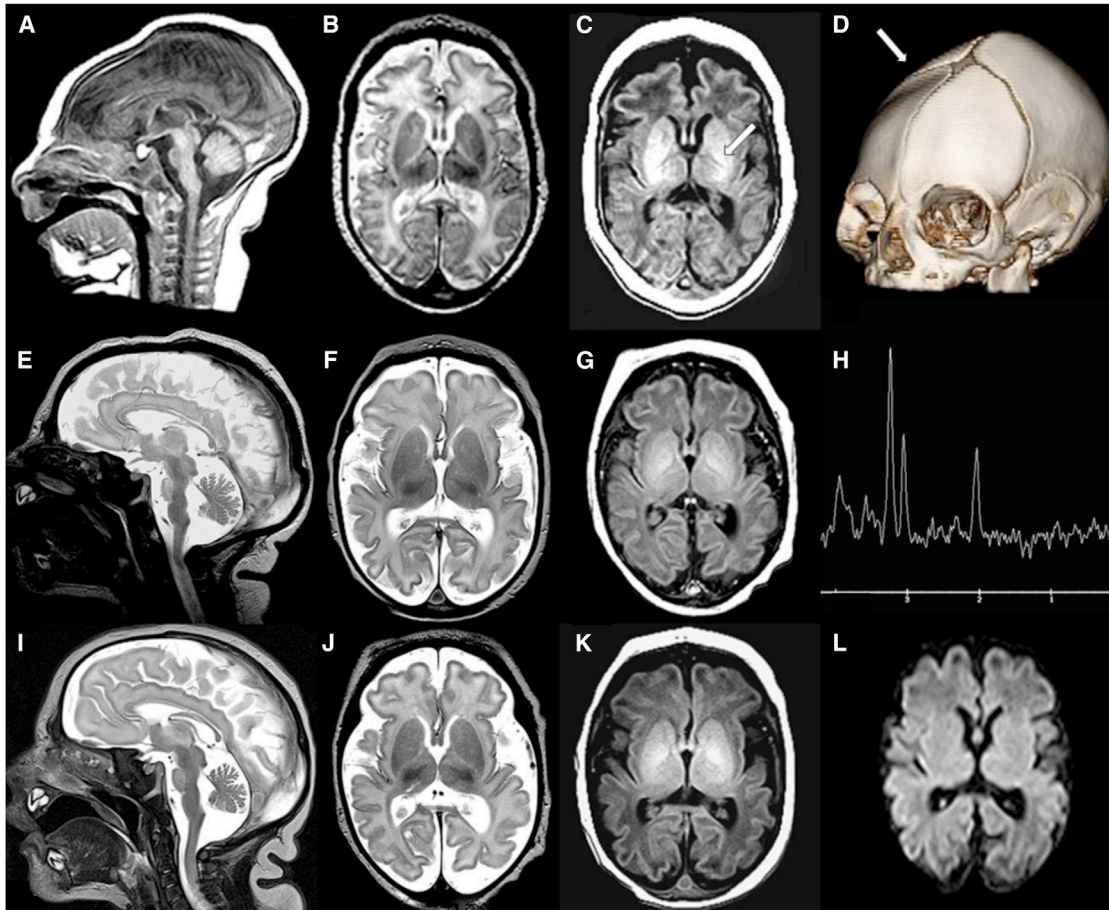


Figure 2. MRI Images from Family C

(A–D) Sibling C.II.1. Sagittal T1W image (A) performed at 13 days of age reveals decreased size of pons. Axial T2W image (B) reveals prominent pericerebral fluid spaces surrounding the brain due to volume loss. White matter is diffusely higher in signal intensity than the cortical ribbon, suggesting delayed myelination. Axial T1W image (C) confirms lack of bright myelin stripe in the posterior limb of internal capsule (arrow). Three-dimensional computed tomography (D) at 2 months of age confirms ridge (arrow) from overlapping sutures, palpable at birth. DNA confirmation was not obtained in this infant.

(E–H) Sibling C.II.3. Sagittal T2W image (E) performed at 6 days of age reveals decreased size of pons. Axial T2W image (F) demonstrates prominent pericerebral fluid spaces surrounding the brain due to volume loss. Axial T1W image (G) confirms lack of myelin stripe in posterior limb of the internal capsule (PLIC). Magnetic resonance spectroscopy (MRS) TE144 (H) performed in the basal ganglia is age appropriate (as it was in all three siblings).

(I–L) Sibling C.II.4. Sagittal T2W image (I) performed at 1 day of age reveals decreased size of pons. Axial T2W image (J) confirms pericerebral fluid prominence due to cerebral volume loss in a manner similar to siblings. Axial T1W image (K) shows lack of myelin stripe in PLIC. Diffusion-weighted imaging (DWI) (L) is normal (as it was in all three siblings).

See also [Figure S1](#).

Family D is a nonconsanguineous French Canadian family, consisting of three affected (D.II.1, D.II.2, and D.II.3) and two unaffected (D.II.4 and D.II.5) siblings ([Figure 1A](#)). Exome sequencing was performed in two affected (D.II.1 and D.II.2) and two unaffected siblings. In total, 237 rare protein or splice-altering variants were present in both affected children (with a frequency $\leq 3\%$ in 169 in-house unrelated exomes, 1,000 Genomes Project data set and data from the NHLBI ESP). We

excluded from this list X-linked variants that were also present in the unaffected male sibling. We also excluded homozygous or possible compound heterozygous variants that were found in the same form in at least one unaffected sibling. Only two variants (c.1648C > T/p.R550C; c.17C > A/p.A6E; NM_183356), both in ASNS, remained after this filtering process ([Table S5](#)).

Critically, in all four families there is complete cosegregation of the identified ASNS mutations/genotypes with disease

Figure 1. Four Families with ASNS Mutations

(A) Cosegregation of mutations within each of the four families. Filled symbols represent known or presumed (in the case of aborted fetus) affected individuals. The individuals with a blue star were exome sequenced.

(B) Sanger sequencing confirmation for all three ASNS mutations in the four families. For family D, Sanger sequencing also confirmed inheritance of each mutation from a different parent (compound heterozygote).

Table 2. Mutations Identified in ASNS

| Family | Genotype | ASNS Modification | Nucleotide Change | Ethnicity | Frequency in Control Exomes/Genomes | Frequency in Ancestry-Matched Controls | PolyPhen-2 | SIFT |
|--------|-----------------------|-------------------|-------------------|-----------------|-------------------------------------|--|------------------|--------------------|
| A | Homozygous | p.F362V | c.1084T>G | Iranian Jewish | 0/261 | 1/80 | Damaging (0.95) | Damaging (0.04) |
| B | Homozygous | p.F362V | c.1084T>G | Iranian Jewish | 0/261 | 1/80 | Damaging (0.95) | Damaging (0.04) |
| C | Homozygous | p.R550C | c.1648C>T | Bangladeshi | 0/169 | 0/225 | Damaging (1.00) | Damaging (0.01) |
| D | Compound heterozygous | p.R550C | c.1648C>T | French Canadian | 0/169 | 0/300 | Damaging (1.00) | Damaging (0.01) |
| | | p.A6E | c.17C>A | | 0/169 | 0/300 | Damaging (0.898) | Deleterious (0.02) |

Nucleotide and amino acid positions are based on the NCBI Reference sequences NM_183356.3 and NP_899199.2, respectively. See also Tables S1–S10.

(Figure 1A). Sanger sequencing was used to validate all three mutations (Figure 1B).

All three missense mutations are predicted to damage the encoded asparagine synthetase protein by available computer algorithms (SIFT and PolyPhen-2) and all three mutations are absent in dbSNP135, the 1,000 Genomes Project data set, and data from the NHLBI ESP (Table 2). To better estimate the frequency of the p.F362V variant in unaffected individuals, we directly genotyped this locus in 1,160 additional controls and failed to detect the mutation. Finally, all three mutations were genotyped in ancestry-matched controls and all remained absent (Table 2), with the exception of p.F362V, which has an estimated carrier frequency of 0.0125 in Iranian Jews.

Additionally, we used the sequence data to test for evidence of cryptic relatedness between the patient in family A and the affected siblings from family B and found no indication of elevated identity by descent beyond what is expected for unrelated genomes (data not shown). We also tested whether the p.F362V ASNS variant is found on a common haplotype in all affected individuals of Iranian Jewish origin. Indeed, the ASNS variant was found on the same 1.2 Mb haplotype in both families and this haplotype was very rare (0.8%) in 261 sequenced controls (Supplemental Experimental Procedures; Table S6). This observation is consistent with a single founder origin for p.F362V and subsequent transmission along with the same extended haplotype. We also did not find evidence for homozygote deletions overlapping the ASNS gene in controls (Supplemental Experimental Procedures).

Interestingly, the mutation p.R550C was found in two families of different ethnic backgrounds. This mutation was associated with different haplotypes in each of these families, suggesting that it arose independently. It should be noted that p.R550C corresponds to a CpG site, which is associated with a higher mutation rate (Nachman and Crowell, 2000), possibly explaining the recurrence of this rare mutation in different populations.

Functional Impact of the Nonsynonymous Mutations

To test the effect of the identified mutations on ASNS mRNA and protein levels, we generated full-length mutant cDNA constructs (p.A6E, p.F362V, and p.R550C) using PCR-mediated site-directed mutagenesis (Figure S2). We then transfected both wild-type and mutant alleles into HEK293 and COS-7 cells and found similarly robust levels of expression of the mRNA corre-

sponding to wild-type and all three mutant alleles (Figure 3A). This result indicates that these mutations do not overtly affect mRNA levels, suggesting that they do not influence mRNA stability. For the p.F362V mutation, we also compared wild-type and mutant full-length transcripts, from the patient fibroblasts, to detect any differences in alternative splicing or exon skipping and found no evidence for alternately spliced transcripts (data not shown).

We used two approaches to detect the ASNS protein in transfected cells. First, we used an antibody to human ASNS (Figure S2). This antibody cross-reacted to produce nonspecific bands and thus we also used C-terminal FLAG-tagged forms of ASNS to detect the wild-type and all three mutant forms of ASNS (Figure S2) using the anti-FLAG antibody. We found that while high levels of the wild-type protein were easily detected, a dramatic reduction in protein abundance was seen in the HEK293 cells expressing the p.A6E or p.F362V mutant allele. In contrast, cells expressing the p.R550C mutant allele had an increased level of protein abundance compared to wild-type (Figure 3B). Consistent with the former observation, a dramatic reduction in ASNS abundance was observed in patient fibroblasts from individual II.1 in family A, harboring the p.F362V allele (Figure S2). This pattern of protein abundance was also observed in COS-7 cells transfected with empty, wild-type, or mutant vectors (Figure S2). These results suggest that these mutations impair ASNS gene function by either reducing protein expression (p.A6E or p.F362V) or reducing functional performance (p.R550C). The mechanism through which the R550C mutation reduces activity remains to be elucidated, but the clinical similarity in presentation of patients suggests that all mutations are loss of function mutations.

We then asked whether these mutations destabilize the protein, targeting it for degradation. We blocked both the ubiquitin-proteasome and the macroautophagy pathways, but neither of these altered ASNS protein abundance (data not shown). We also used Leupeptin to inhibit lysosomal-dependent degradation and this also failed to rescue the p.A6E or p.F362V mutant proteins to wild-type levels (Figure 3B), although some experiments did show a trend toward rescue (data not shown).

ASNS encodes the glutamine-dependent asparagine synthetase enzyme (EC 6.3.5.4), which catalyzes ammonia transfer from glutamine to aspartic acid via a β -aspartyl-AMP intermediate. Concordant with this biochemical function, we found that

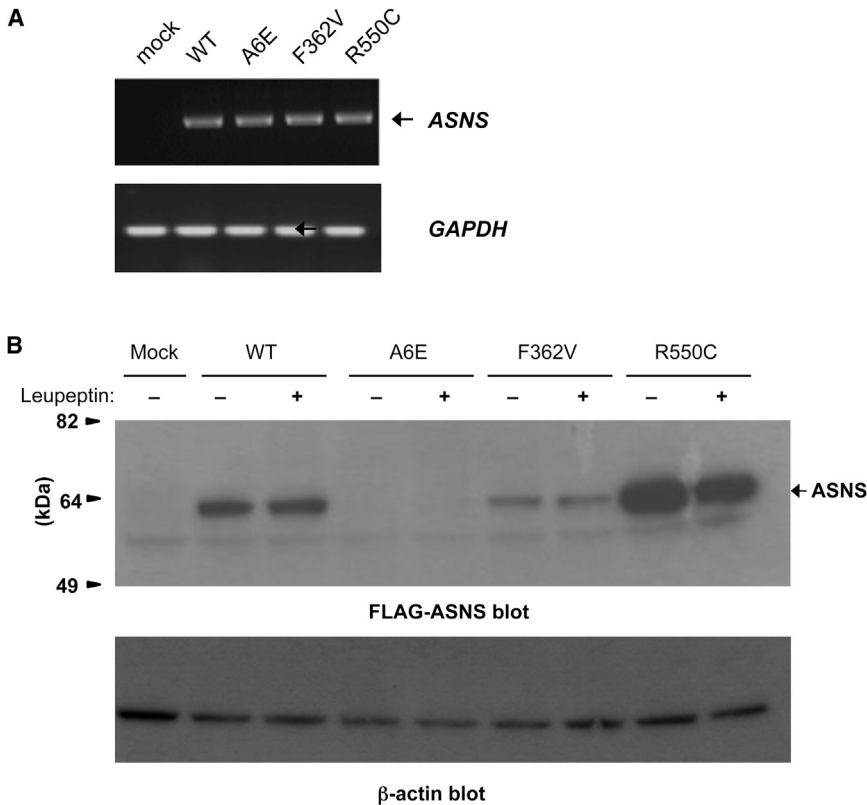


Figure 3. Functional Impact of ASNS Mutations

(A) RT-PCR to detect ASNS mRNA expression in COS-7 cells transfected with empty, wild-type, or mutant vectors.

(B) Western blots detecting ASNS-FLAG protein abundance, with or without Leupeptin treatment, in the HEK293 transfectants using an anti-FLAG antibody. β -actin was used as a loading control. See also Figure S2.

the levels of asparagine were decreased in at least two affected individuals (C.II.3 and D.II.1), whereas glutamine and aspartic acid, both precursors in the ASNS-catalyzed synthesis of asparagine, were mildly elevated in the patients from family B (Table 3). These findings are consistent with our in vitro functional studies, emphasizing that the identified mutations have phenotypic consequences.

The mutated amino acid residues in ASNS are located within regions of high sequence conservation among orthologs, from bacterium to man (Figure 4A), indicating that these amino acids are likely to be critical for protein function. This is further supported by the inferred positions of the human ASNS mutations in the folded bacterial ortholog (Figure 4B; Supplemental Experimental Procedures).

ASNS Expression in the Brain

Cells are capable of both nutritional intake and endogenous synthesis of asparagine, suggesting that ASNS may be dispensable, and raising the question of how loss of ASNS protein or its dysfunction results in a severe, tissue-specific phenotype. ASNS is under complex transcriptional regulation (Chen et al., 2004; Greco et al., 1989; Li et al., 2006; Richards and Kilberg, 2006) and is expressed at low levels in most tissues but is highly expressed in the adult brain, with evidence for a brain-specific splice variant(s) (Figure S3) (Hongo et al., 1996). Consistent with this expression pattern, *Asns* is expressed in the adult mouse brain (Allen Brain Atlas). In situ hybridization shows that *Asns* is also expressed in the developing embryonic mouse brain (E14.5), is particularly enriched in the cortical plate where the

neurons reside, and is also expressed in the ventricular and subventricular zone layers (VZ and SVZ) lining the ventricles of the cerebral cortex, where neural progenitors reside (Figure S3) (Visel et al., 2004). RNA-seq of E14.5 cortices also confirms this pattern of expression in the cortical plate and VZ (Ayoub et al., 2011). This expression pattern is similar to that of known microcephaly genes (Bond et al., 2002; Jackson et al., 2002), consistent with a role for *Asns* in cortical development and brain size.

Asns Gene-Trap Mice

We obtained genetically modified mice from EUCOMM in which the *Asns* genomic locus contains a gene-trap insertion in intron 2 (ENSMUST00000115542) containing a splice acceptor site and the LacZ gene (B6NTac;B6N-*Asns*^{tm1a(EUCOMM)Wtsj/H}, termed *Asns*^{-/-}; Figure S4).

Gene traps are frequently hypomorphs, as there can be splicing that skips over the gene-trap cassette, but the degree to which this splicing occurs is construct and gene specific (Adams and van der Weyden, 2008). To determine the extent of *Asns* expression in the *Asns* gene-trap mice, we performed a comprehensive *Asns* mRNA analysis in the brains (cerebral hemispheres) of adult *Asns*^{+/+}, *Asns*^{+/-}, and *Asns*^{-/-} mice (3 to 4 months of age). First, RT-PCR was used to semiquantitatively assess the existence of *Asns* mRNA transcripts. RT-PCR spanning from the second exon to the last exon (exon 12) revealed a single band the size of the expected wild-type *Asns* transcript in all three genotypes (Figure S4). These bands were gel purified and Sanger sequenced, which confirmed that the wild-type transcript was present in all three genotypes and no aberrant splicing events were observed. Additionally, *Gapdh* RT-PCR was performed as an internal control and the homozygous mice show a decreased abundance of the wild-type *Asns* transcript compared to the wild-type mice (Figure S4). To quantify this difference, we performed quantitative real-time TaqMan PCR using a probe spanning exons seven and eight. The mRNA levels were significantly different between the three genotypes (one-way ANOVA; $p < 0.00001$) (Figure 5A). A post hoc two-tailed t test revealed that both mutant genotypes were significantly different from wild-type mRNA levels ($P_{Asns(+/+)-Asns(+/-)} = 0.00001$, $*P_{Asns(+/+)-Asns(-/-)} < 0.00001$) and significantly different

Table 3. Measurements of Amino Acid Concentrations in Patient Blood and Urine

| | Plasma Amino Acid Levels | | | Urine Amino Acid Levels | | |
|--------|------------------------------------|------------------------------|--------------------------------|--|---|---|
| | Glutamine | Aspartate | Asparagine | Glutamine | Aspartate | Asparagine |
| B.II.2 | 1,250 (254–823 $\mu\text{mol/l}$) | 18 (1–24 $\mu\text{mol/l}$) | 57 (23–112 $\mu\text{mol/l}$) | 382 (20–112 $\mu\text{mol}/\text{mmol creatinine}$) | 36 (1–10 $\mu\text{mol}/\text{mmol creatinine}$) | 21 (0–24 $\mu\text{mol}/\text{mmol creatinine}$) |
| B.II.4 | 1,149 (254–823 $\mu\text{mol/l}$) | 2 (1–24 $\mu\text{mol/l}$) | 49 (23–112 $\mu\text{mol/l}$) | 57 (20–112 $\mu\text{mol}/\text{mmol creatinine}$) | 40 (1–10 $\mu\text{mol}/\text{mmol creatinine}$) | 4 (0–24 $\mu\text{mol}/\text{mmol creatinine}$) |
| C.II.1 | NA | 7 (17–21 $\mu\text{mol/l}$) | NA | NA | NA | NA |
| C.II.3 | NA | NA | 12 (16–21 $\mu\text{mol/l}$) | NA | NA | NA |
| C.II.4 | NA | 12 (0–20 $\mu\text{mol/l}$) | NA | NA | NA | NA |
| D.II.1 | 439 (474–736 $\mu\text{mol/l}$) | 7 (4–18 $\mu\text{mol/l}$) | 11 (31–56 $\mu\text{mol/l}$) | NA | NA | NA |
| D.II.2 | 668 (474–736 $\mu\text{mol/l}$) | 9 (4–18 $\mu\text{mol/l}$) | 55 (31–56 $\mu\text{mol/l}$) | NA | NA | NA |

Data were not available for all fields in all patients (NA). The reference concentrations are indicated within parentheses. See also [Table S11](#).

from each other ($*P_{Asns(+/-)-Asns(-/-)} = 0.00083$). We were unable to determine whether there was differential expression of the *Asns* protein, due to lack of quality and specific mouse anti-*Asns* antibodies. These data demonstrate that the *Asns* gene-trap mouse is a hypomorph with $\sim 20\%$ of the normal level of *Asns* mRNA being expressed. Given that two of the human mutations lead to decreased protein expression, this mouse provides a reliable model for this phenotype.

We next analyzed the brains of *Asns*^{-/-} and control (*Asns*^{+/+} or *Asns*^{+/-}) littermates from embryos and adults. We obtained coronal sections from postnatal day (P) 0 brains and measured cortical area, cortical thickness, and lateral ventricle area for each mouse using rostral-caudal-matched sections (using anatomical landmarks). We found that the cortical thickness and area of the *Asns*^{-/-} brains were, on average, $\sim 14\%$ thinner and $\sim 5\%$ smaller than their control littermates, respectively. Additionally, the lateral ventricle area in the *Asns*^{-/-} mice was significantly larger than their control littermates ($p = 0.019$; [Figure S4](#)).

Due to the progressive nature of the human disorder, we next evaluated whether adults showed exacerbated brain defects. We generated paraffin-embedded coronal sections from P84 brains of *Asns*^{-/-} and *Asns*^{+/-} littermates (three of each genotype) (representative sections shown in [Figure S4](#)). The use of heterozygous animals was considered suitable because human carriers of ASNS mutations remain unaffected. We analyzed rostral-caudal-matched sections (using anatomical landmarks) from each animal for several parameters. Measurement of the cortical surface area, using methods described by Pulvers and colleagues ([Pulvers et al., 2010](#)), showed an $\sim 8\%$ reduction in cortical surface area of *Asns*^{-/-} mice ([Figure 5B](#)). A similar reduction ($\sim 5\%$) was observed in the whole-brain surface area of *Asns*^{-/-} mice ([Figure 5C](#)). We also observed that the *Asns*^{-/-} brains had increased lateral ventricles ($\sim 95\%$) relative to control brains ([Figure 5D](#)). Importantly, the cortical thickness of the *Asns*^{-/-} mice was significantly reduced compared to the *Asns*^{+/-} mice ($p = 0.022$; [Figure 5E](#)).

Asns^{+/-} and *Asns*^{-/-} mice were assessed with age-matched B6NTac control animals in four behavioral assays. We found no genotype-associated differences in spontaneous locomotor activity, performance on the rotarod, or anxiety-like behavior in the light-dark emergence test; however, *Asns*^{+/-} mice were defi-

cient and *Asns*^{-/-} mice were severely impaired in short- and long-term memory in the novel object recognition task ([Supplemental Experimental Procedures](#); [Figure S5](#)).

Careful observations of mice during behavioral testing revealed no evidence of seizure activity. To examine the possibility that *Asns*^{-/-} mice might display epileptiform activity, we conducted prolonged video electroencephalogram (EEG) recordings in chronically implanted *Asns*^{-/-} mice ($n = 2$) and a wild-type (WT) control ($n = 1$). Neither behavioral nor electrographic seizures were detected in *Asns*^{-/-} mice or the WT controls.

Taken together, these data indicate that this *Asns* mouse model recapitulates the human brain phenotype, particularly in the reduced cortical thickness and increased lateral ventricle area.

DISCUSSION

We report that mutations in asparagine synthetase (ASNS) cause a distinct neurodevelopmental disorder characterized by congenital microcephaly, profound intellectual disability, and progressive cerebral atrophy. We found that two of these mutations reduce the abundance of the protein. Finally, we have shown that disrupting this gene in mice creates a model that mimics aspects of the human phenotype, including structural brain abnormalities and learning deficits, albeit with what appears to be a generally milder presentation than observed in humans.

Studies performed on cancer cells showed that asparagine depletion affects cell proliferation and survival (reviewed in [Richards and Kilberg, 2006](#)). This is classically illustrated by the effect of asparaginase administration in childhood acute lymphoblastic leukemia. Asparaginase delivery to the bloodstream results in asparagine depletion causing a rapid efflux of cellular asparagine, which is also destroyed. Most cells express sufficient ASNS to counteract this asparagine starvation and survive, but not leukemic cells. Similarly, loss of ASNS activity in thermosensitive mutant BHK cells leads to cell-cycle arrest as a consequence of a depletion of cellular asparagine ([Greco et al., 1989](#); [Li et al., 2006](#)).

During development, *Asns* is expressed in regions where both neural progenitors and postmitotic neurons are present,

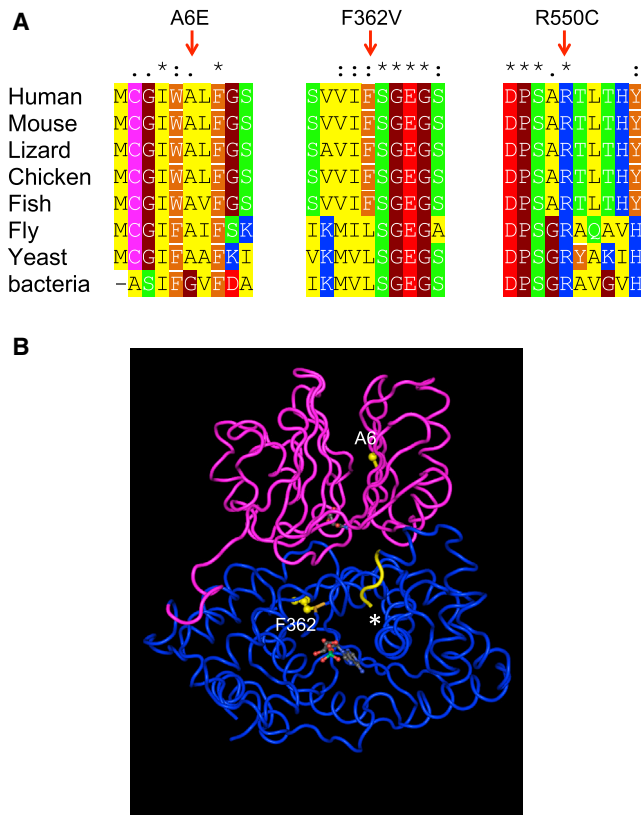


Figure 4. Location and Conservation of Mutated Residues in the ASNS Gene

(A) A multiple alignment of human ASNS and selected orthologs. Only the regions harboring mutations are shown. On top: “*” represents identical position; “:” represents conserved substitutions; “.” represents semiconserved substitution. Color code is for amino acid type: red, negative; blue, positive; green, polar; yellow, aliphatic; orange, aromatic; brown, helix breaker.

(B) The structure of *E. coli* glutamine-dependent asparagine synthetase B (protein databank ID 1CT9), a bacterial ortholog of human ASNS (A). The N-terminal glutamine aminotransferase domain is colored in pink, and the C-terminal asparagine synthase domain is colored in blue. The residues inferred to be equivalent to the mutated A6E and F362V are highlighted in yellow and the approximate location of the mutated R550C is shown with an asterisk (crystallography could not be determined for the distal end of C-terminal domain). Also, the AMP and glutamine molecules are shown in space-filling style.

suggesting that it may function in either or both of these populations. A subset of the brains from our subjects had simplified gyri. Similar features were found in the mutant mice, which showed decreased cortical thickness and enlarged lateral ventricles. These structural abnormalities could be caused in part by aberrations in neural progenitor proliferation during development, resulting from decreased asparagine levels. Asparagine depletion could also cause increased cell death in postmitotic neurons or glial cells, contributing to the progressive atrophy of the brain observed in our subjects.

Strikingly, ASNS deficiency causes severe neurological impairment, without any involvement of peripheral tissues. The concentration of asparagine in the cerebrospinal fluid (CSF) of humans is only ~10% of the concentration found in plasma

(Scholl-Bürgi et al., 2008). The poor transport of asparagine across the blood-brain barrier suggests that the brain depends on local de novo synthesis, explaining why the phenotype is essentially neurological.

In addition to ID, a subset of our patients presented with features of hyperexcitability (including epilepsy and hyperekplexia). These features suggest a mechanism that is consistent with the accumulation of aspartate/glutamate in the brain, resulting in enhanced excitability and neuronal damage. While seizures in the patients could reflect enhanced excitability, these could also be secondary to the structural effects of altered proliferation. We cannot exclude the possibility that multiple mechanisms may be contributing to the observed human phenotype. Further analyses of animal and cellular models will help to elucidate the function of ASNS in normal brain development.

Of particular interest is the observation that *Asns* hypomorphic mice appear to have a milder phenotype than the humans with regards to more modest structural effects on the brain and no evidence of seizures. The ratio for the concentration of asparagine in the CSF to plasma in rats (0.26) (Nishimura et al., 1995) appears to be slightly elevated compared to that of humans (0.081 [Akiyama et al., 2012] to 0.118 [Scholl-Bürgi et al., 2008]). Assuming that the CSF/plasma ratio is similar in mouse and rat, this suggests that the concentration of asparagine is increased in the CSF and interstitial fluid (ISF) of mouse/rat as compared to humans. Thus, asparagine may be more readily available to the *Asns*^{-/-} mice due to some physiological difference between humans and mice, such as transport at the blood-brain barrier. Alternately, it is possible that low levels of *Asns* expression in these mice result in a less severe phenotype. It will be of great interest to compare the hypomorph to a complete *Asns* null animal, which may show an even more dramatic phenotype.

With this report, ASNS deficiency becomes the third example of a recently recognized group of conditions resulting from the inability to synthesize a nonessential amino acid. These conditions all feature severe congenital encephalopathy with microcephaly. The others are glutamine synthetase deficiency (Häberle et al., 2005) and the serine biosynthetic disorders (van der Crabben et al., 2013). Although knowledge of ASNS deficiency and of other inborn errors of nonessential amino acid synthesis is incomplete, general considerations regarding diagnosis, disease mechanism, and treatment are in order. In almost every respect, the clinical approach to these diseases is predicted to be the opposite of that recommended for classical amino acidopathies, which are caused by deficient breakdown of essential amino acids.

Strikingly, every diagnosis of ASNS deficiency was made by molecular genetics, despite extensive previous evaluation of patients that in several cases included amino acid chromatography of plasma and CSF. Why was ASNS deficiency not suspected on these grounds? The answer may lie in a combination of technical considerations and biology. Compared to most amino acids, the normal levels of asparagine are low, both in plasma (e.g., 50.7 ± 17.7 μmol/l, in children 0–3 years old) and CSF (e.g., 4.0 ± 2.9 μmol/l) (Akiyama et al., 2012; Scholl-Bürgi et al., 2008). For many reasons, low levels of a metabolite may be less evident than increases. Abnormally low levels are more

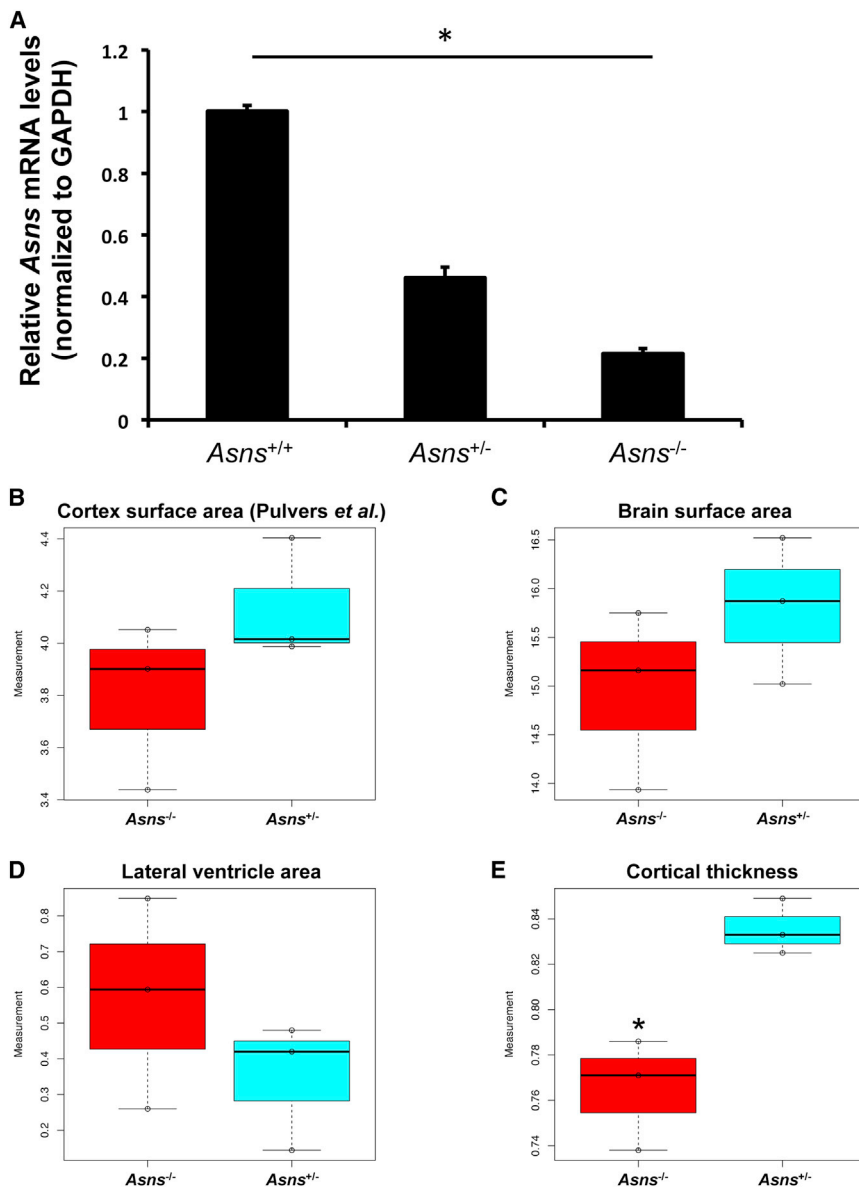


Figure 5. *Asns*-Deficient Mice and Structural Brain Abnormalities

(A) Detection of *Asns* mRNA (qRT-PCR) in the mouse brain. Four mice of each genotype were used (all 3–4 months of age). The expression differences between the three genotypes are significant (one-way ANOVA test $*p < 0.00001$). A post hoc two-tailed t test revealed both mutant genotypes were significantly different from wild-type expression ($P_{Asns(+/-)-Asns(+/-)} = 0.00001$, $*P_{Asns(+/-)-Asns(-/-)} < 0.00001$) and significantly different from each other ($*P_{Asns(+/-)-Asns(-/-)} = 0.00083$). Error bars represent SEM.

(B–E) Measurements of adult mouse brain (P84) coronal sections, analyzed using ImageJ software (Schneider et al., 2012), comparing three homozygous mutants to heterozygous littermates. (B) Cortical surface area as measured in Pulvers et al. (2010). (C) Surface area of the left hemisphere of the brain section, (D) surface area of the lateral ventricle in the left hemisphere of the brain section, and (E) cortical thickness measured from the edge of the hippocampus to the outer cortex. Asterisk (*) indicates a significant difference by an unpaired t test ($p = 0.022$). Error bars represent the range of the observed data.

See also Figures S3, S4, and S5.

deficient amino acid becomes essential. Hence, an obvious first consideration for therapy is dietary supplementation, to provide the deficient amino acid to the brain. Plasma levels can usually be substantially increased by dietary supplementation and despite the complex transport systems for amino acids at the brain endothelium, a therapeutic benefit of supplementation has been reported in serine biosynthetic disorders and glutamine synthetase deficiency (van der Crabben et al., 2013; Häberle et al., 2012). Supplementation with asparagine therefore seems reasonable

easily concealed by variations due to physiological state such as nutrition (which is difficult to standardize in ill newborns or infants) and to machine performance in diagnostic laboratories. In fact, currently used diagnostic technologies cannot discriminate low from normal CSF asparagine levels. In summary, results to date suggest that in patients with unexplained congenital encephalopathy with microcephaly, the absence of a low value does not exclude ASNS deficiency. In the future, an enzyme assay may play an important role in the complete diagnostic evaluation of patients suspected of ASNS deficiency but experience is too limited to conclude. In children with severe congenital encephalopathy and microcephaly, ASNS deficiency should be considered, and molecular diagnosis is the only method with proven reliability.

All three known deficiencies of amino acid biosynthesis present mainly with neurological features. In these conditions, the

in ASNS deficiency. However, the prenatal onset of the microcephaly and the early postnatal presentation raise the possibility that such treatment will not be curative unless started prenatally.

The *Asns* mouse we have analyzed here will provide a model for future comprehensive exploration of the factors influencing phenotypic severity. Comparing this hypomorphic mouse model with a null mouse model will allow us to directly evaluate how residual levels of ASNS activity compare with the absence of ASNS activity, which may inform us about differences in clinical presentation. We can also utilize both animal models when testing the effects of dietary supplementation, which would ensure that a range of ASNS activities were represented, thus covering the full range of ASNS activities that may also occur in patients. This work therefore sets the stage for evaluation of treatment options in *Asns* mouse models.

Early diagnosis of ASNS deficiency is now possible. Careful clinical observations and studies of ASNS-deficient mice will help define the clinical spectrum and resolve central unanswered issues regarding the pathophysiology of this condition.

EXPERIMENTAL PROCEDURES

Recruitment of Subjects and Collection of Samples

Families A and B were recruited at Sheba and Wolfson Medical Centers in Israel, family C at The Hospital for Sick Children in Toronto (Canada), and family D at Sainte-Justine Hospital in Montreal (Canada). Blood samples were obtained from most affected individuals, their unaffected siblings, and their parents. The relevant Institutional Review Boards approved the studies and appropriate family members gave written consent.

Sequencing and Variant Identification

Exome Sequencing in Families A and B

The Illumina Genome Analyzer Ix platform (Illumina) was used to perform exome sequencing of the three sequenced microcephaly patients (Figure 1, family A: II.1 and family B: II.2 and II.4) at the Center for Human Genome Variation (CHGV) at Duke University, Durham, NC. Prior to sequencing, target regions were captured using the SureSelect Human All Exon technology (Agilent Technologies). This technology captures consensus coding sequence exonic regions and flanking intronic regions totaling ~38 Mb of genomic DNA. The resulting short-sequence reads were aligned to the reference genome (NCBI human genome assembly build 36; Ensembl core database release 50.361 [Hubbard et al., 2009]) using the Burrows-Wheeler Alignment (BWA) tool (Li and Durbin, 2009). After accounting for PCR duplicates (removed using the Picard software: <http://picard.sourceforge.net>) and reads that did not align to captured regions of the reference genome, the average coverage for these three samples was ~71× and each sample had >95% of the bases covered. A base within the 37.8 Mb captured region was defined as covered if ≥5 short reads spanned this nucleotide (Table S10).

Genetic differences between each patient genome and the reference genome were identified using the SAMtools variant calling program (Li et al., 2009), which identifies both single-nucleotide variants (SNVs) and small indels. We then used the SequenceVariantAnalyzer software (SVA) (Ge et al., 2011) to annotate all identified variants. SVA was also used to apply quality control filters to the variants identified by SAMtools. High-quality SNVs were obtained using the following criteria: consensus score ≥20, SNP quality score ≥20, and reads supporting SNP ≥3. High-quality indels were obtained using the following criteria: consensus score ≥20, indel quality score ≥50, ratio of (reads supporting variant/reads supporting reference): 0.2–5.0, and reads supporting indel ≥3.

Exome Sequencing in Families C and D

The exomes of one of the individuals of family C (II.3) and four individuals of family D (II.1, II.2, II.4, and II.5) were captured using the Agilent SureSelect all exon kit V3 (approximately 51.9 Mb of target sequences) and then sequenced in pair ends (2 × 100 bp) on the Illumina HiSeq2000 (v3 chemistry; 3 exomes/lane format) at the McGill University Genome Quebec Innovation Center (Montreal, Canada). The sequences were aligned and the variants were called using GATK (DePristo et al., 2011). After removal of duplicate reads, using Picard, we obtained an average coverage of >80× per target base, with 95% of the target bases being covered at ≥10×. Only variants that meet all the following criteria were considered: base coverage ≥8×, reads supporting the variant ≥3, and ratio of reads supporting variant/reads supporting reference ≥20%. Variants were then annotated using Annovar (Wang et al., 2010).

Genotyping p. F362V

Genotyping of the p.F362V variant in 1,160 controls was performed in the Center for Human Genome Variation at Duke University (Durham, NC). This was done using a custom TaqMan genotyping assay (Applied Biosystems): forward: 5'-CCTGCGTAAGTTCATCTGATCCTT-3'; reverse: 5'-GTATATTCGGAAGAACACAGATAGCGT-3'; probe: 5'-TCCAGAGA[A/C]GATCACC-3'.

Genotyping of the p.F362V variant in 80 Iranian Jewish controls and the non-exome-sequenced family members (Figure 1; family A: I.1, I.2, II.2, II.3, and II.4

and family B: I.1, I.2, II.1) was performed at the Gertner Institute of Human Genetics, Sheba Medical Center, Israel. Sanger Sequencing (Figure 1B) or restriction digest with the restriction enzyme Alw26I (data not shown) were used to perform this genotyping. Both methods used the following custom primer sequences: forward: 5'-CTTCAATTATTTCCAAAAATCAAATC-3' and reverse: 5'-CACTGCATACTGAAAGATGATAGAAA-3'. These primers resulted in a 286 bp amplicon that targeted the nucleotide of interest.

The p.F362V variant, found in families A and B, was validated in these three samples using all three methods: TaqMan genotyping, Sanger sequencing, and restriction digestion.

Genotyping p.R550C and p.A6E in French Canadian and Bangladeshi Controls

Sanger sequencing of PCR-amplified products was used to genotype p.R550C and p.A6E variants. The following custom primers were used for p.A6E: forward: 5'-GCCGTTGAATGTAGAGGTC-3' and reverse: 5'-CCAAAGCAGCAGTTGGTGA-3'. The following custom primers were used for p.R550C: forward: 5'-GCCATTTAAGCCATTTTGC-3' and reverse: 5'-TTTCCCTTTTCTAGCTTACC-3'. The mutations p.R550C and p.A6E were genotyped in 300 French Canadian healthy controls. In addition, p.R550C was genotyped in 225 Bangladeshi healthy controls.

Clone Preparations

Full-length cDNA encoding human ASNS was amplified from first-strand cDNA derived from the HEK293 human kidney cell line with an RNeasy plus mini kit (QIAGEN), High Capacity cDNA Reverse Transcription Kit (Applied Biosystems), Phusion HF DNA polymerase (Finnzymes), and a specific primer set (5'-CTCGAGATGTGTGGCATTGGGCGCT-3' and 5'-CTCGAGCC TAAGCTTTGACAGCTGACT-3'). The cDNA was subcloned into the pCR-Blunt II-TOPO vector (Invitrogen-Life Technologies) and subjected to sequence analysis (pCR-Blunt II-ASNS-WT). Using pCR-Blunt II-ASNS-WT, A6E, F362V, and R550C of ASNS were made by PCR-mediated site-directed mutagenesis using Phusion HF DNA polymerase and a specific primer set (A6E: 5'-GCTGTTGGCAGTGATGATTG-3' and 5'-TCCCAAATGCCACACATCTC-3'; F362V: 5'-GTCTCTGGAGAAGGATCAGA-3' and 5'-GATCACCAGCTATC TGTGT-3'; R550C: 5'-GCACGCTGACCCACTAC-3' and 5'-AGGCAGAAG GGTCAGTGC-3'), which were phosphorylated by T4 polynucleotide kinase (New England Biolabs). The amplicons were self-ligated using T4 DNA ligase (Promega) and subjected to sequence analysis (pCR-Blunt II-ASNS-A6E, pCR-Blunt II-ASNS-F362V, and pCR-Blunt II-ASNS-R550C). ASNS human cDNA containing each allele was subcloned into the pcDNA3.1(+) vector (Invitrogen-Life Technologies) using the KpnI and XbaI sites from pCR-Blunt II-ASNS-WT, pCR-Blunt II-ASNS-A6E, pCR-Blunt II-ASNS-F362V, or pCR-Blunt II-ASNS-R550C and subjected to sequence analysis (pcDNA3.1(+)-ASNS-WT, pcDNA3.1(+)-ASNS-A6E, pcDNA3.1(+)-ASNS-F362V, or pcDNA3.1(+)-ASNS-R550C; Figure S2).

Using pcDNA3.1(+)-ASNS-WT, pcDNA3.1(+)-ASNS-A6E, pcDNA3.1(+)-ASNS-F362V, or pcDNA3.1(+)-ASNS-R550C, FLAG-tagged-modified ASNS was made by two-step PCR-mediated site-directed mutagenesis using Phusion HF DNA polymerase and specific primer sets (first step: 5'-GACAAG TAGGCTCGAGAAGGG-3' and 5'-GTAGTCAGCTTTGACAGCTGAC-3'; second step: 5'-GACGATGACAAGTAGGCTCGAGAAGGG-3' and 5'-GTCCTTG TAGTCAGCTTTGACAG-3'), which were phosphorylated by T4 polynucleotide kinase, the amplicons were self-ligated using T4 DNA ligase and subjected to sequence analysis (pcDNA3.1(+)-ASNS-FLAG-WT, pcDNA3.1(+)-ASNS-FLAG-A6E, pcDNA3.1(+)-ASNS-FLAG-F362V, or pcDNA3.1(+)-ASNS-FLAG-R550C). cDNAs encoding FLAG-tagged human ASNS were subcloned into pcDNA3.1(+) vector again, using the KpnI and XbaI sites and subjected to sequence analysis (Figure S2).

Cell Culture: RT-PCR

Empty pcDNA3.1(+) vector, pcDNA3.1(+)-ASNS wild-type, or pcDNA3.1(+)-ASNS mutant (p.F362V, p.R550C, or p.A6E) were transfected into the monkey COS-7 kidney cell line or human HEK293 kidney cells by lipofection using Lipofectamine 2000 (Invitrogen-Life Technologies). Total RNA was extracted from transfectants using an RNeasy plus mini kit, and first-strand full-length cDNA encoding human ASNS was synthesized using the High Capacity cDNA Reverse Transcription Kit (Applied Biosystems). RT-PCR to detect ASNS mRNA expression was performed in 25 cycles at 96°C for 30 s, 60°C for 30 s, and 72°C for 30 s using AmpliTaq Gold DNA polymerase (Applied

Biosystems) and a specific primer set (5'-TGACGCCCTCTATGACAAT-3' and 5'-CACCTTTCTAGCAGCCAGTA-3') (Figure 3A).

Cell Culture: Western Blotting

Forty-eight hours after transfection, the cells were lysed with RIPA buffer (Sigma-Aldrich) with Protease inhibitor cocktail (Sigma-Aldrich), and the lysates were subjected to SDS-PAGE gel and transferred to a polyvinylidene difluoride membrane (Millipore). The membranes were incubated with anti-FLAG M2 monoclonal antibody (Sigma-Aldrich) or anti-actin antibody (Santa Cruz Biotechnology). Proteins were visualized with the ECL plus western blotting detection system (GE Healthcare). For Leupeptin treatment, 24 hr posttransfection, the cells were incubated with 100 μ M Leupeptin (Sigma Aldrich). After 8 hr incubation with Leupeptin, the cells were lysed, and FLAG-tagged ASNS were detected as above.

Protein Conservation

Species and ASNS proteins were from gi P08243 (Human, *Homo sapiens*), ENSMUSP00000031766 (mouse, *Mus musculus*), ENSGALP00000015846, (chicken, *Gallus gallus*), ENSACAP00000012780 (lizard, *Anolis carolinensis*), ENSXETP00000054608, (frog, *Xenopus tropicalis*), ENSTRUP00000013503 (fish, fugu, *Takifugu rubripes*), FBpp0089009 (fruit fly, *Drosophila melanogaster*), NP_741864 (worm, nematode, *Caenorhabditis elegans*), YGR124W (yeast, *Saccharomyces cerevisiae*), and YP_003233213.1 (bacterium, *Escherichia coli*) (Figure 4A). Sequence alignment was performed using ClustalW (Thompson et al., 2002) and alignment editing with the BioEdit software (<http://www.mbio.ncsu.edu/bioedit/bioedit.html>).

The pdb structure was made using Discovery Studio program (<http://accelrys.com/products/discovery-studio>) (Figure 4B).

Mouse Analyses

Asns mice were obtained from the Eucomm consortium. Mice were maintained by breeding to C57BL/6NTac. Histology at P0 was performed by cryopreservation of tissue, cryosectioning, and hematoxylin and eosin staining. Histology in adult brains was performed by fixation of tissue using formalin perfusion. Tissue was sent to <http://www.histoserv.com> for paraffin embedding, sectioning, and staining. Analysis of area and thickness was performed by quantifying measurements using ImageJ. The p values for structural measurements were obtained using an unpaired t test and calculations were done using R.

cDNA

Mouse cerebral hemispheres were carefully dissected. Total RNA was extracted from brain tissue using an RNeasy plus mini kit, and first-strand full-length cDNA encoding human ASNS was synthesized using the High Capacity cDNA Reverse Transcription Kit (Applied Biosystems).

Quantitative Real-Time RT-PCR

Quantitative real-time PCR was done using an *Asns* gene expression assay, with FAM reporter, spanning exons 7–8 (Mm00803785_m1; Life Technologies) and a *Gapdh* gene expression assay with VIC reporter (Mm9999915_g1; Life Technologies). Samples were run in triplicate and the standard curve was made using cDNA from a nontest wild-type sample. Twelve mice between 3 and 4 months of age were used for qPCR. Four mice of each genotype were used (*Asns*^{+/+}, *Asns*^{+/-}, and *Asns*^{-/-}). One-way ANOVA was used to assess expression differences between the three genotypes ($p < 0.00001$). A post hoc two-tailed t test was then used to assess genotypic differences in expression ($P_{WT-Asns^{+/-}} = 0.00001$, $*P_{WT-Asns^{-/-}} < 0.00001$, $*P_{Asns^{+/-} - Asns^{-/-}} = 0.00083$).

Regular RT-PCR

RT-PCR to detect *Asns* mRNA expression was performed in 35 cycles at 96°C for 30 s, 58°C for 30 s, and 72°C for 90 s using AmpliTaq Gold DNA polymerase (Applied Biosystems) and a specific primer set (5'-CAGTGTCTGAGTGCGATGAAGA-3' and 5'-GCGTTCAAAGATCTGACGGTAG-3') (Figure S4).

RT-PCR to detect *Gapdh* mRNA expression was performed in 25 cycles at 96°C for 30 s, 57°C for 30 s, and 72°C for 45 s using AmpliTaq Gold DNA polymerase (Applied Biosystems) and a specific primer set (5'-ACCACAGTCATGCCATCAC-3' and 5'-CACCACCTGTTGCTGTAGCC-3') (Figure S4).

Western Blotting

Two different antibodies were tried for detection of mouse Asns: anti-human ASNS, which recognizes amino acid residues 506–520 of ASNS (Sigma-Aldrich), and anti-Asns, with species reactivity in mouse, rat, and human, which recognizes amino acid residues at the C terminus (Abcam). Both were nonspecific (data not shown).

Video EEG Recordings of Mice

Two adult *Asns* homozygous mice and one age-matched WT mouse were anesthetized by intraperitoneal injection of Nembutal (60 mg/kg). Under stereotaxic guidance, four monopolar electrodes were implanted into the subdural space over the left and right parietal cortex and occipital cortex for chronic EEG recording. After a 7-day postoperative recovery, EEG activity was recorded with the mouse moving freely in a cage for 80 hr; animal behavior was recorded simultaneously with a digital video camera. The EEG and behavioral activities were analyzed by an individual blinded to mouse genotype.

SUPPLEMENTAL INFORMATION

Supplemental Information includes Supplemental Experimental Procedures, five figures, and 11 tables and can be found with this article online at <http://dx.doi.org/10.1016/j.neuron.2013.08.013>.

ACKNOWLEDGMENTS

We would like to thank all four families for their willingness to participate in this study. J.L.M. is a National Scientist of the Fonds de Recherche en Santé. E.K.R. is funded by a predoctoral grant from the Epilepsy Foundation and the Jo Rae Wright Fellowship for outstanding women in science (Duke University). J.M.C.-C. holds a salary award from the Réseau de Médecine Génétique Appliquée du Québec (RMGA). We acknowledge the following colleagues for supplying control samples: R. Brown, G. Cavalleri, L. Cirulli, N. Delanty, C. Depondt, V. Dixon, E. Heinzen, J. Hoover-Fong, A. Husain, D. Levy, K. Linney, W. Lowe, J. McEvoy, M. Mikati, J. Milner, A. Need, R. Ottman, R. Radtke, J. Silver, M. Silver, S. Sisodiya, N. Sobriera, D. Valle, and N. Walley. We wish to thank Katherine Whang for helping to section the mouse brains. We wish to thank C. Means and T. Rhodes for helping with the behavioral experiments and J. Zhou and C. Elms for breeding, genotyping, and maintaining the mice. We thank R. Olender and P. Allard for helpful insights. We also thank the members of the RMGA bioinformatic team (Alexandre Dionne-Laporte, Dan Spiegelman, Edouard Henrion, and Ousmane Diallo) for the bioinformatic analysis of the exome sequencing data (families C and D). This research has been funded in part by federal funds from the Center for HIV/AIDS Vaccine Immunology ("CHAVI") under a grant from the National Institute of Allergy and Infectious Diseases, National Institutes of Health, Grant Number U01AI067854 to D.B.G., and by the March of Dimes (grant no. 12-FY10-236) and Canadian Institutes of Health Research (MOP 106499) to J.L.M. Additional funding provided by: ARRA 1RC2NS070342-01, NIMH Grant RC2MH089915, NINDS Award RC2NS070344, and the Crown Human Genome Center at the Weizmann Institute of Science.

Accepted: August 15, 2013

Published: October 16, 2013

REFERENCES

- Adams, D.J., and van der Weyden, L. (2008). Contemporary approaches for modifying the mouse genome. *Physiol. Genomics* 34, 225–238.
- Adzhubei, I.A., Schmidt, S., Peshkin, L., Ramensky, V.E., Gerasimova, A., Bork, P., Kondrashov, A.S., and Sunyaev, S.R. (2010). A method and server for predicting damaging missense mutations. *Nat. Methods* 7, 248–249.
- Akiyama, T., Kobayashi, K., Higashikage, A., Sato, J., and Yoshinaga, H. (2012). CSF/plasma ratios of amino acids: Reference data and transports in children. *Brain Dev.* Published online December 31, 2012. <http://dx.doi.org/10.1016/j.braindev.2012.12.001>.
- Ayoub, A.E., Oh, S., Xie, Y., Leng, J., Cotney, J., Dominguez, M.H., Noonan, J.P., and Rakic, P. (2011). Transcriptional programs in transient embryonic zones of the cerebral cortex defined by high-resolution mRNA sequencing. *Proc. Natl. Acad. Sci. USA* 108, 14950–14955.
- Bond, J., Roberts, E., Mochida, G.H., Hampshire, D.J., Scott, S., Askham, J.M., Springell, K., Mahadevan, M., Crow, Y.J., Markham, A.F., et al. (2002). ASPM is a major determinant of cerebral cortical size. *Nat. Genet.* 32, 316–320.

- Chen, H., Pan, Y.X., Dudenhausen, E.E., and Kilberg, M.S. (2004). Amino acid deprivation induces the transcription rate of the human asparagine synthetase gene through a timed program of expression and promoter binding of nutrient-responsive basic region/leucine zipper transcription factors as well as localized histone acetylation. *J. Biol. Chem.* 279, 50829–50839.
- DePristo, M.A., Banks, E., Poplin, R., Garimella, K.V., Maguire, J.R., Hartl, C., Philippakis, A.A., del Angel, G., Rivas, M.A., Hanna, M., et al. (2011). A framework for variation discovery and genotyping using next-generation DNA sequencing data. *Nat. Genet.* 43, 491–498.
- Ge, D., Ruzzo, E.K., Shianna, K.V., He, M., Pelak, K., Heinzen, E.L., Need, A.C., Cirulli, E.T., Maia, J.M., Dickson, S.P., et al. (2011). SVA: software for annotating and visualizing sequenced human genomes. *Bioinformatics* 27, 1998–2000.
- Greco, A., Gong, S.S., Ittmann, M., and Basilico, C. (1989). Organization and expression of the cell cycle gene, ts11, that encodes asparagine synthetase. *Mol. Cell. Biol.* 9, 2350–2359.
- Häberle, J., Görg, B., Rutsch, F., Schmidt, E., Toutain, A., Benoist, J.-F., Gelot, A., Suc, A.-L., Höhne, W., Schliess, F., et al. (2005). Congenital glutamine deficiency with glutamine synthetase mutations. *N. Engl. J. Med.* 353, 1926–1933.
- Häberle, J., Shahbeck, N., Ibrahim, K., Schmitt, B., Scheer, I., O’Gorman, R., Chaudhry, F.A., and Ben-Omran, T. (2012). Glutamine supplementation in a child with inherited GS deficiency improves the clinical status and partially corrects the peripheral and central amino acid imbalance. *Orphanet J. Rare Dis.* 7, 48.
- Hongo, S., Chiyo, T., and Takeda, M. (1996). Cloning of cDNA for asparagine synthetase from rat Sertoli cell. *Biochem. Mol. Biol. Int.* 38, 189–196.
- Hubbard, T.J.P., Aken, B.L., Ayling, S., Ballester, B., Beal, K., Bragin, E., Brent, S., Chen, Y., Clapham, P., Clarke, L., et al. (2009). Ensembl 2009. *Nucleic Acids Res.* 37(Database issue), D690–D697.
- Jackson, A.P., Eastwood, H., Bell, S.M., Adu, J., Toomes, C., Carr, I.M., Roberts, E., Hampshire, D.J., Crow, Y.J., Mighell, A.J., et al. (2002). Identification of microcephalin, a protein implicated in determining the size of the human brain. *Am. J. Hum. Genet.* 71, 136–142.
- Li, B.S., Gu, L.J., Luo, C.Y., Li, W.S., Jiang, L.M., Shen, S.H., Jiang, H., Shen, S.H., Zhang, B., Chen, J., et al. (2006). The downregulation of asparagine synthetase expression can increase the sensitivity of cells resistant to l-asparaginase. *Leukemia* 20, 2199–2201.
- Li, H., and Durbin, R. (2009). Fast and accurate short read alignment with Burrows-Wheeler transform. *Bioinformatics* 25, 1754–1760.
- Li, H., Handsaker, B., Wysoker, A., Fennell, T., Ruan, J., Homer, N., Marth, G., Abecasis, G., and Durbin, R.; 1000 Genome Project Data Processing Subgroup. (2009). The Sequence alignment/map format and SAMtools. *Bioinformatics* 25, 2078–2079.
- Mahmood, S., Ahmad, W., and Hassan, M.J. (2011). Autosomal Recessive Primary Microcephaly (MCPH): clinical manifestations, genetic heterogeneity and mutation continuum. *Orphanet J. Rare Dis.* 6, 39.
- Nachman, M.W., and Crowell, S.L. (2000). Estimate of the mutation rate per nucleotide in humans. *Genetics* 156, 297–304.
- Ng, P.C., and Henikoff, S. (2003). SIFT: Predicting amino acid changes that affect protein function. *Nucleic Acids Res.* 31, 3812–3814.
- Nishimura, F., Nishihara, M., Mori, M., Torii, K., and Takahashi, M. (1995). Excitability of neurons in the ventromedial nucleus in rat hypothalamic slices: modulation by amino acids at cerebrospinal fluid levels. *Brain Res.* 691, 217–222.
- Pulvers, J.N., Bryk, J., Fish, J.L., Wilsch-Bräuninger, M., Arai, Y., Schreier, D., Naumann, R., Helppi, J., Habermann, B., Vogt, J., et al. (2010). Mutations in mouse *Aspm* (abnormal spindle-like microcephaly associated) cause not only microcephaly but also major defects in the germline. *Proc. Natl. Acad. Sci. USA* 107, 16595–16600.
- Richards, N.G.J., and Kilberg, M.S. (2006). Asparagine synthetase chemotherapy. *Annu. Rev. Biochem.* 75, 629–654.
- Schneider, C.A., Rasband, W.S., and Eliceiri, K.W. (2012). NIH image to ImageJ: 25 years of image analysis. *Nat. Methods* 9, 671–675.
- Scholl-Bürgi, S., Haberlandt, E., Heinz-Erian, P., Deisenhammer, F., Albrecht, U., Sigl, S.B., Rauchenzauner, M., Ulmer, H., and Karall, D. (2008). Amino acid cerebrospinal fluid/plasma ratios in children: influence of age, gender, and antiepileptic medication. *Pediatrics* 121, e920–e926.
- Thompson, J.D., Gibson, T.J., and Higgins, D.G. (2002). Multiple sequence alignment using ClustalW and ClustalX. *Curr. Protoc. Bioinformatics Chapter 2*, <http://dx.doi.org/10.1002/0471250953.bi0203s00>, Unit 2.3.
- van der Crabben, S.N., Verhoeven-Duif, N.M., Brilstra, E.H., Van Maldergem, L., Coskun, T., Rubio-Gozalbo, E., Berger, R., and de Koning, T.J. (2013). An update on serine deficiency disorders. *J. Inher. Metab. Dis.* 36, 613–619.
- Visel, A., Thaller, C., and Eichele, G. (2004). GenePaint.org: an atlas of gene expression patterns in the mouse embryo. *Nucleic Acids Res.* 32(Database issue), D552–D556.
- Wang, K., Li, M., and Hakonarson, H. (2010). ANNOVAR: functional annotation of genetic variants from high-throughput sequencing data. *Nucleic Acids Res.* 38, e164.